Invited Feature Article

One-Dimensional Nanostructures of Metals: Large-Scale Synthesis and Some Potential Applications

Jingyi Chen,† Benjamin J. Wiley,‡ and Younan Xia*,†

Departments of Chemistry and Chemical Engineering, University of Washington, Seattle, Washington 98195

Received November 1, 2006. In Final Form: December 10, 2006

We review recent developments in our group regarding the solution-phase synthesis of one-dimensional nanostructures of metals. The synthetic approaches include solution−liquid−solid growth for nanowires of low-melting-point metals such as Pb; seed-directed growth for Ag nanowires, nanobeams, and nanobelts; kinetically controlled growth for Pt nanorods, nanowires, and multipods; and galvanic replacement for nanotubes of Au, Pt, and Pd. Both characterization and mechanistic studies are presented for each nanostructure. Finally, we highlight the electrical and plasmonic properties of these metal nanostructures and discuss their potential applications in nanoscale devices.

Introduction

One-dimensional (1-D) nanostructures are slivers of material constrained in two dimensions to less than 100 nm.[1] Within this category of nanomaterials, researchers discriminate between nanorods with aspect ratios (length/diameter) less than 10, nanowires with aspect ratios greater than 10, and nanotubes with hollow interiors. Research on nanostructures is primarily guided by three questions: (i) how can we produce large quantities of nanostructures with controllable sizes and shapes; (ii) what are the size- and shape-dependent physical properties of nanostructures; and (iii) how can the properties unique to nanostructures be exploited for applications? Pursuing answers to these questions has evolved into an active field of research now commonly referred to as nanoscience and nanotechnology.[2] Since the genesis of this field in the 1980s, it has grown to such colossal proportions that no succinct summary can be given; a large amount of effort has been devoted to nanowire-related research alone.[3]

Here we focus on our own work regarding the solution-phase synthesis of 1-D nanostructures of metals, including the characterization of their physical properties and the demonstration of potential applications. To date, we have successfully synthesized 1-D nanostructures from Pb, Ag, Au, Pt, and Pd. These metals all have a face-centered cubic (fcc) structure, and thus no crystallographic driving force for anisotropic growth. Indeed, thermodynamics dictates that to minimize their surface energy, atoms of these metals should assemble to form faceted spheres (e.g., single-crystal cuboctahedrons) rather than nanowires.[4] That is why any solution-phase synthesis of 1-D nanostructures of metals involves not only a solvent, metal precursor, and reducing agent but also a surfactant, polymer, or ionic species capable of modifying the kinetics of atom assembly to generate shapes other than thermodynamically favored spheres.[5]

It is critical to have fine control over the dimensions of a nanostructure because this parameter largely determines its properties and applications. For example, the color of gold and silver nanorods can be readily tuned from the visible to the near-infrared region by increasing their aspect ratios.[6] Metal nanorods that scatter light in the visible can serve as tunable optical labels.[7] Those that absorb in the near-infrared can be used for photothermal therapy.[8] The long lengths of nanorods or nanowires increase the likelihood that they will contact each other, making them ideal fillers for thermally and electrically conductive polymer composites.[9] Suspensions of nanowires can be sprayed for EM shielding or nanoscale electrical interconnects.[10] Studies on the physical properties of metal nanowires have already advanced

* Corresponding author. E-mail: xia@chem.washington.edu.
† Department of Chemistry.
‡ Department of Chemical Engineering.

(1) Xia, Y.; Yang, P.; Sun, Y.; Wu, Y.; Mayers, B.; Gates, B.; Yin, Y.; Kim, F.; Yan, H. *Adv. Mater.* **2003**, *15*, 353.

(2) See, for example, (a) Ozin, G. A.; Arsenault, A. C. *Nanochemistry: A Chemical Approach to Nanomaterials*; RSC Publishing: Cambridge, U.K., 2006. (b) *Introduction to Nanoscale Science and Technology*; Di Ventra, M., Evoy, S., Heflin, J. R., Eds.; Kluwer Academic Publishers: Norwell, MA, 2004. (c) *Handbook of Nanostructured Materials and Nanotechnology*; Nalwa, H. S., Ed.; Academic Press: New York, 2000. (d) *Nanomaterials: Synthesis, Properties, and Applications*; Edelstein, A. S., Cammarata, R. C., Eds.; Institute of Physics: Philadelphia, PA, 1996.

(3) See, for example, *Nanowires and Nanobelts: Materials, Properties, and Devices*; Wang, Z. L., Ed.; Kluwer Academic Publishers: Norwell, MA, 2003.

(4) (a) Pimpinelli, A.; Villain J. *Physics of Crystal Growth*; Cambridge University Press: Cambridge, U.K., 1998. (b) Wulff, G. *Z. Kristallogr.* **1901**, *34*, 449. (c) Holden, A.; Singer, P. *Crystals and Crystal Growing*; Doubleday & Company, Inc.: Garden City, NY, 1960.

(5) (a) Yin, Y.; Alivisatos, A. P. *Nature* **2005**, *437*, 26. (b) Murphy, C. J.; Sau, T. K.; Gole, A.; Orendorff, C. J. *MRS Bull.* **2005**, *30*, 349. (c) Lee, S.-M.; Cho, S.-N.; Cheon, J. *Adv. Mater.* **2003**, *15*, 441. (d) Peng, X. *Adv. Mater.* **2003**, *15*, 459.

(6) Recent reviews: (a) Hu, M.; Chen, J.; Li, Z.-Y.; Au, L.; Hartland, G. V.; Li, X.; Marquez, M.; Xia, Y. *Chem. Soc. Rev.* **2006**, *35*, 1084. (b) Eutis, S.; El-Sayed, M. A. *Chem. Soc. Rev.* **2006**, *35*, 209. (c) Pérez-Juste, J.; Pastoriza-Santos, I.; Liz-Marzán, L. M.; Mulvaney, P. *Coord. Chem. Rev.* **2005**, *249*, 1870.

(7) (a) Oldenburg, A. L.; Hansen, M. N.; Zweifel, D. A.; Wei, A.; Boppart, S. A. *Opt. Express* **2006**, *14*, 6724. (b) Orendorff, C. J.; Baxter, S. C.; Goldsmith, E. C.; Murphy, C. J. *Nanotechnology* **2005**, *16*, 2601. (c) Alekseeva, A. V.; Bogatyrev, V. A.; Dykman, L. A.; Khlebtsov, B. N.; Trachuk, L. A.; Melnikov, A. G.; Khlebtsov, N. *Appl. Opt.* **2005**, *44*, 6285. (d) Keating, C. D.; Natan, M. J. *Adv. Mater.* **2003**, *15*, 451.

(8) (a) Huang, X.; El-Sayed, I. H.; Qian, W.; El-Sayed, M. A. *J. Am. Chem. Soc.* **2006**, *128*, 2116. (b) Wang, H.; Huff, T. B.; Zweifel, D. A.; He, W.; Low, P. S.; Wei, A.; Cheng, J.-X. *Proc. Natl. Acad. Sci. U.S.A.* **2005**, *102*, 15752.

(9) Carmona, F.; Barreau, F.; Delhaes, P.; Canet, R. *J. Phys. Lett.* **1980**, *41*, L-531.

(10) (a) Gardner, C. L.; Apps, R.; Russell, A. J. *High Power Microwaves* **1995**, *1*, 12. (b) Lee, C. Y.; Song, H. G.; Jang, K. S.; Oh, E. J.; Epstein, A. J.; Joo, J. *Synth. Met.* **1999**, *102*, 1346.

10.1021/la063193y CCC: $37.00
Published on Web 01/24/2007

our fundamental understanding of size-dependent transport for electrons, photons, and phonons.[11] In contrast, many opportunities remain for studying the physical properties of metal nanotubes and for testing their suitability as electrodes, biosensors, or conduits in nanofluidic devices.[12] In the last section of this feature article, we highlight our own studies of superconducting lead nanowires as well as electronic and plasmonic transport through 1-D nanostructures of silver.

Synthetic Approaches to 1-D Nanostructures of Metals

Perhaps the most conceptually simple way to generate a 1-D nanostructure is to confine its growth with a template. The nanoscale channels in polycarbonate and alumina membranes have been most widely used for this purpose,[13] but 1-D nanostructures can also be grown inside mesoporous silica,[14] cylindrical micelles,[15] and block copolymers[16] as well as along an edge or groove on a solid surface.[17] In many cases, the template needs to be removed in a postsynthesis step so the nanostructures can be put to use. In general, template-based methods cannot be easily scaled up to produce nanostructures quickly and cheaply for commercial applications.

This realization has led our group to pursue solution-phase synthesis capable of producing uniform 1-D nanostructures in large quantities. For the growth of nanorods and nanowires, we rely on an inexpensive solvent, ethylene glycol, that when heated also acts as a reducing agent. In addition, we add poly(vinyl pyrrolidone) (PVP, commonly used in toothpaste and hair spray), to prevent aggregation and guide anisotropic growth. Below we discuss how this polyol process has served as a generic method for the large-scale synthesis of 1-D nanostructures of Pb, Ag, and Pt. We further show how Ag nanowires can be transformed into nanotubes made of Au, Pd, or Pt through a galvanic replacement reaction in an aqueous or organic medium. For each type of nanostructure, detailed electron microscopy studies are provided to help illuminate the mechanism of formation.

Solution−Liquid−Solid Growth and Pb Nanowires. The solution−liquid−solid (SLS) method was originally developed for generating single-crystal semiconductor nanowires in the solution phase at relatively low temperatures.[18] In a typical process, atoms and/or small clusters from the decomposition of an organometallic compound enter nanoscale droplets of a catalyst metal and then nucleate/grow into single-crystal nanorods and nanowires. By analogy to this process, we have demonstrated the large-scale synthesis of single-crystal lead nanowires with diameters in the range of 50−90 nm and lengths of up to several millimeters by thermally decomposing lead acetate in boiling ethylene glycol.[19] In this case, Pb atoms resulting from the decomposition of lead acetate first condense into nanoscale droplets, after which some of them continue to grow and evolve into micrometer-sized crystals. In the last step, Pb nanowires nucleate and grow from the corners of the microcrystals at the expense of nanoscale Pb droplets remaining in the solution phase, as driven by Ostwald ripening.[20]

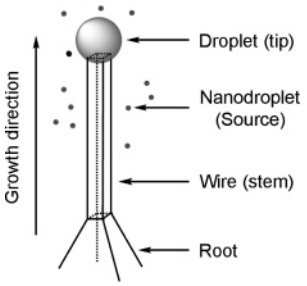

Figure 1. Schematic illustrating the growth of a Pb nanowire with three main components: root, stem, and tip. The Pb nanodroplets in the solution phase serve as the source of atoms for growth. As a result of Ostwald ripening, the Pb atoms leave the surface of the nanodroplet and enter the large droplet, providing a continuous supply of Pb atoms for nanowire growth.

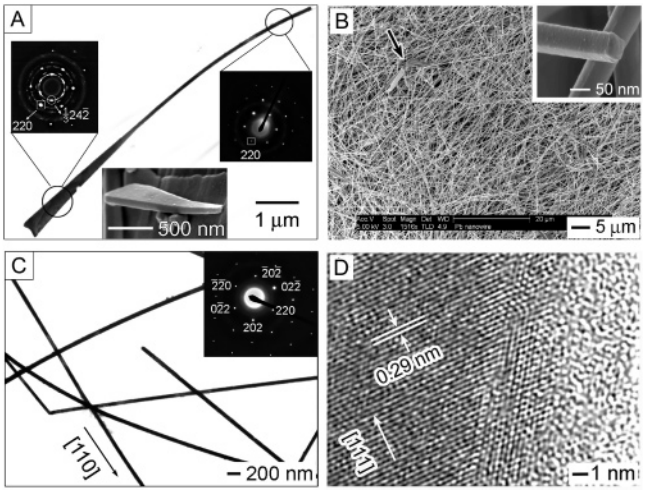

Figure 2. (A) TEM image of an individual Pb nanowire and the ED patterns (insets) taken from its root and stem, respectively. The inset also shows the side-view SEM image of another wire in its early stage of growth, indicating that both the root and stem of this wire were confined to the same plane. (B) SEM image of as-synthesized Pb nanowires demonstrating the uniformity in diameter (∼85 nm) and length up to several millimeters. The inset shows the cross-section of a broken nanowire. (C) TEM image of the Pb nanowires shown in B. The inset gives the ED pattern taken from an individual nanowire. (D) High-resolution TEM image recorded from the edge of a Pb nanowire.

Figure 1 shows a schematic of the growth mechanism.[19a] The Pb nanowire is composed of three segments: root, stem, and tip. The micrometer-sized crystal serves as the root to initiate the nucleation and growth of a nanowire. Because of lead's relatively low melting point, Pb atoms from the solution phase are attracted to the reactive site and form a small droplet at the tip. Once the size of the droplet at the tip has reached a critical value, the Pb atoms start to crystallize at the interface between the tip and the root to form the stem. As more and more Pb atoms are driven into the tip, the stem continues to grow into a uniform nanowire until all of the Pb source droplets in the solution phase have been depleted. This mechanism is in agreement with both TEM and SEM observations. Figure 2A shows the TEM image of a typical nanowire, together with two electron diffraction (ED) patterns

(11) (a) Lieber, C. M. *Solid State Commun.* **1998**, *107*, 607. (b) Prokes, S. M.; Wang, K. L. *MRS Bull.* **1999**, *24*, 13.
(12) Goldberger, J.; Fan, R.; Yang, P. *Acc. Chem. Res.* **2006**, *39*, 239.
(13) (a) Martin, C. R. *Science* **1994**, *266*, 1961. (b) Martin, B. R.; Dermody, C. J.; Reiss, B. D.; Fang, M.; Lyon, L. A.; Natan, M. J.; Mallouk, T. E. *Adv. Mater.* **1999**, *11*, 1021.
(14) (a) Lee, K.-B.; Lee, S.-M.; Cheon, J. *Adv. Mater.* **2001**, *294*, 348. (b) Han, Y.; Kim, J.; Stucky, G. D. *Chem. Mater.* **2000**, *12*, 2068. (c) Hunag, M. H.; Choudrey, A.; Yang, P. *Chem. Commun.* **2000**, 1063.
(15) Kijima, T.; Yoshimura, T.; Uota, M.; Ikeda, T.; Fujikawa, D.; Mouri, S.; Uoyama, S. *Angew. Chem., Int. Ed.* **2004**, *43*, 228.
(16) Cornelissen, J. J. L. M.; Van Heerbeek, R.; Kamer, P. C. J.; Reek, J. N. H.; Sommerdijk, N. A. M.; Nolte, R. J. M. *Adv. Mater.* **2002**, *14*, 489.
(17) (a) Penner, R. M. *J. Phys. Chem. B* **2002**, *106*, 3339. (b) Jones, E. T. T.; Chyan, O. M.; Wrighton, M. S. *J. Am. Chem. Soc.* **1987**, *109*, 5526. (c) Bishop, D. J.; Licini, J. C.; Dolan, G. J. *Appl. Phys. Lett.* **1985**, *46*, 1000.
(18) (a) Holmes, J. D.; Johnston, K. P.; Doty, R. C.; Korgel, B. A. *Science* **2000**, *287*, 1471. (b) Trentler, T. J.; Hickman, K. M.; Geol, S. C.; Viano, A. M.; Gibbons, P. C.; Buhro, W. E. *Science* **1995**, *270*, 1791.
(19) (a) Wang, Y.; Jiang, X.; Herricks, T.; Xia, Y. *J. Phys. Chem. B* **2004**, *108*, 8631. (b) Wang, Y.; Herricks, T.; Xia, Y. *Nano Lett.* **2003**, *3*, 1163.
(20) Roosen, A.; Carter, W. *Physica A* **1998**, *261*, 232.

taken from its root and stem portions, respectively. Both ED patterns exhibit 6-fold symmetry recorded along the [111] zone axis of this fcc crystal. Another set of spots located in the center region of the ED pattern of the root (as marked by a circle) could be attributed to the (1/3){422} reflection that is forbidden for an fcc lattice. The appearance of these forbidden spots was often associated with thin structures that were enclosed by atomically flat top and bottom facets.[21] The inset at the bottom gives an oblique SEM image of the root portion of a nanowire in its early stage of growth. It is clear that the root displayed planar or platelike morphology and the growth of the nanowire was initiated from the thinner end of the plate.

Using this simple approach, we can easily produce Pb nanowires in large quantities. Figure 2B shows the SEM image of a typical sample of Pb nanowires that are 85 ± 5 nm in diameter and up to several millimeters in length. The inset gives an enlarged view of the end of a fractured nanowire, indicating a rectangular cross-section. As indicated by an arrow, there is a small amount of platelike structure in the product that served as the roots. Figure 2C shows a TEM image of the nanowires. The inset gives an ED pattern taken from an individual nanowire with the electron beam being oriented along the [$\bar{1}$11] axis, indicating that the wire grew along the [110] axis. The diffraction pattern was essentially unchanged as the electron beam was scanned across each individual nanowire, suggesting that they were single crystals. These results are also consistent with the HRTEM image that was taken from the edge of a nanowire, as shown in Figure 2D. The lattice spacing was measured to be 0.29 nm, which matched the spacing between the {111} planes of fcc lead.

The yield of Pb nanowires in a typical synthesis was determined by two major factors: the amount of PVP and the temperature. The ratio of PVP to lead acetate had to be around 3.5 in order to obtain a 100% yield of nanowires. When any value other than 3.5 was used, the main products were found to be belts and thin plates. It is also important to keep the reaction temperature higher than 190 °C to thermally decompose lead acetate and generate Pb atoms. Otherwise, only lead salts were found in the reaction product. Interestingly, the reaction direction showed a strong dependence on temperature. At the boiling temperature of ethylene glycol, the thermal decomposition of lead acetate was favored, and Pb atoms could be formed in 90 min. The Pb atoms were converted back to lead salt in 10 min when the reaction mixture was cooled. When the temperature was increased, Pb atoms became the dominant species again, leading to the formation of Pb nanowires as the final product. In general, the Pb nanowires have to be protected from oxidation under an inert gas. The availability of uniform Pb nanowires provides us an opportunity to exploit their electron-transport properties at reduced dimensions. This synthetic route based on the SLS growth mechanism can likely be extended to other metals with relatively low melting points, including bismuth, tin, cadmium, and their alloys.

Seed-Directed Growth of Silver Nanowires, Nanobeams, and Nanobelts. As Ag^+ ions are reduced to atoms in solution, they come together to form nuclei with fluctuating structures.[22] Most nuclei incorporate twin boundary defects to minimize their surface energy.[23] As nuclei grow, fluctuations cease, and a distribution of single-crystal, singly twinned, and multiply twinned seeds form, with the 5-fold-twinned decahedron being one of the lowest energy and most abundant species. We have demonstrated that these decahedron seeds grow into silver nanowires with a pentagonal cross-section under the confinement of PVP.[24] In this process, silver nitrate was reduced by ethylene glycol in the presence of PVP, chloride, and iron. The addition of chloride at a ratio of 1 to every 500 silver atoms electrostatically stabilized seeds against aggregation, whereas a micromolar concentration of iron ions prevented oxidative etching.[25] In the growth step, Ag atoms preferentially crystallize on the twin defects (the highest energy sites), leading to uniaxial elongation of the decahedron into a pentagonal nanorod. As shown in Figure 3A, the side surface of such a nanorod is bound by {100} facets. Because PVP interacts more strongly with the {100} facets than with the {111} facets, both ends of the nanorod remain accessible toward the incoming Ag atoms whereas the side surface is completely passivated by PVP (Figure 3B).[24] As a result, the nanorod can readily grow into a long nanowire with a uniform cross-section along the nanowire axis.

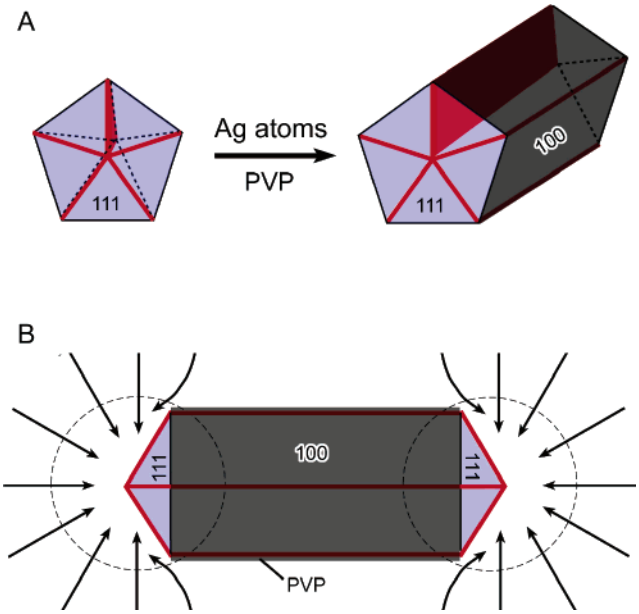

Figure 3. Schematic illustrating the growth mechanism for Ag nanowires: (A) Evolution of a nanorod from a multiply twinned nanopraticle (MTP) of silver. The ends of the nanorod are terminated by {111} facets with pentagonal symmetry, and the side surfaces are bounded by {100} facets. (B) Projection perpendicular to one of the five side facets of a nanorod showing the diffusion of Ag atoms toward both ends of this nanorod indicated by the arrows, with the side surfaces completely passivated by PVP.

Figure 4A shows the SEM image of a typical sample of Ag nanowires with lengths up to tens of micrometers. The inset is an SEM image of a nanowire intentionally broken by sonication for 1 h, clearly showing its pentagonal cross-section and flat edges. This observation is supported by the TEM images taken from a microtomed sample of Ag nanowires. As shown in Figure 4B, most of the cross-sections exhibited a pentagonal shape with 5-fold symmetry. The non-pentagonal cross-sections could be attributed to the random orientations of Ag nanowires relative to the edge of the microtome knife and the coexistence of a very small number of Ag colloidal particles in the as-synthesized sample. The inset gives a TEM image clearly showing the twin

(21) (a) Allpress, J.; Sanders, J. *Surf. Sci.* **1967**, *7*, 1. (b) Kirkland, A. I.; Jefferson, D. A.; Duff, D. G.; Edwards, P. P.; Gameson, I.; Johnson, B. F. G.; Smith, D. J. *Proc. R. Soc. London, Ser. A* **1993**, *440*, 589. (c) Germain, V.; Li, J.; Ingert, D.; Wang, Z. L.; Pileni, M. P. *J. Phys. Chem. B* **2003**, *107*, 8717.

(22) Smith, D. J.; Petford-Long, A. K.; Wallenberg, L. R.; Bovin, J. O. *Science* **1986**, *233*, 872.

(23) Ajayan, P. M.; Marks, L. D. *Phys. Rev. Lett.* **1998**, *60*, 585.

(24) (a) Sun, Y.; Gates, B.; Mayers, B.; Xia, Y. *Nano Lett.* **2002**, *2*, 165. (b) Sun, Y.; Yin, Y.; Mayers, B.; Herricks, T.; Xia, Y. *Chem. Mater.* **2002**, *14*, 4736. (c) Sun, Y.; Xia, Y. *Adv. Mater.* **2002**, *14*, 833. (d) Sun, Y.; Mayers, B.; Herricks, T.; Xia, Y. *Nano Lett.* **2003**, *3*, 955.

(25) Wiley, B.; Sun, Y.; Xia, Y. *Langmuir* **2005**, *21*, 8077.

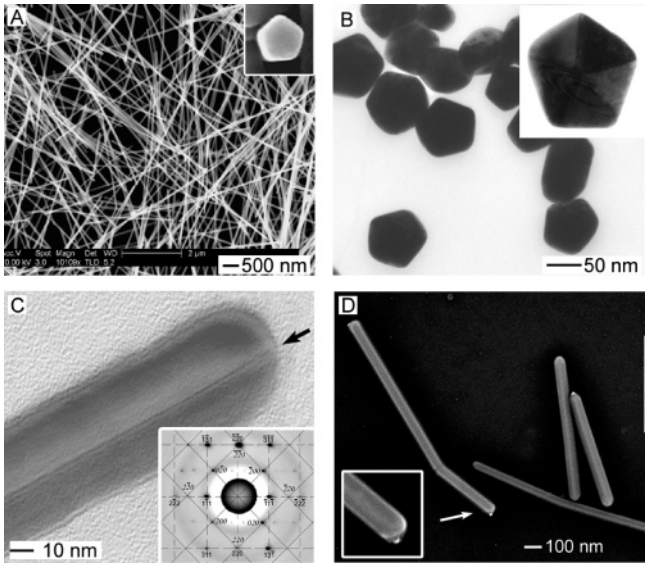

Figure 4. (A) SEM image of Ag nanowires with a uniform diameter (∼50 nm) along the entire nanowire length. The inset shows the cross-section of a broken nanowire. (B) TEM image of a microtomed sample of the nanowires shown in A, indicating the pentagonal symmetry of their cross-sections. The inset gives a TEM image at a slightly higher magnification, confirming that each wire has a fivefold twinned structure. (C) TEM image taken from the end of an individual nanowire, showing the existence of a twin plane along its longitudinal axis (as indicated by the arrow). The inset gives an SAED pattern taken from an individual nanowire by aligning the electron beam perpendicular to one of the {100} facets. (D) SEM image of Ag nanowires after they had been reacted with 1,12-dodecanedithiol, followed by incubation with Au nanoparticles for 10 h. The Au nanoparticles were found as bright dots only at the ends of the nanowires, suggesting that the side surfaces were blocked by PVP coverage.

boundaries between the five single-crystal subunits. Figure 4C shows a TEM image recorded from the end of a Ag nanowire, showing a twin plane oriented parallel to its longitudinal axis, as indicated by the arrow. The inset shows the typical ED pattern recorded from an individual nanowire by aligning the electron beam perpendicular to the wire. The diffraction spots could be divided into two sets: ones with square symmetry corresponding to the [001] zone axis and those with rectangular symmetry corresponding to the $[1\bar{1}\bar{2}]$ zone axis. The remaining spots were attributed to double diffraction from the mutual orientation of these two zones. These assignments were consistent with the results obtained from multiply twinned nanorods of Au and Cu with the same pentagonal symmetry and {100} side facets.[26]

To examine further the interaction between PVP and different facets of silver, the nanowires were incubated in a dilute solution of 1,12-dodecanedithiol for 1 h and then with Au nanoparticles (prepared by reducing $HAuCl_4$ with sodium citrate) for another 10 h. The dithiol molecules allow the gold nanoparticles to attach to the surface of the Ag nanowires. Figure 4D shows an SEM image of the final product in which Ag nanowires were decorated with Au nanoparticles on their ends but not their sides. This observation suggested that PVP interacted more strongly with the {100} facets than with the {111} facets and dithiol molecules could be chemically adsorbed only on the ends of a nanowire. It is worth noting that Au nanoparticles also readily attached to the fresh surface created whenever a nanowire was broken.

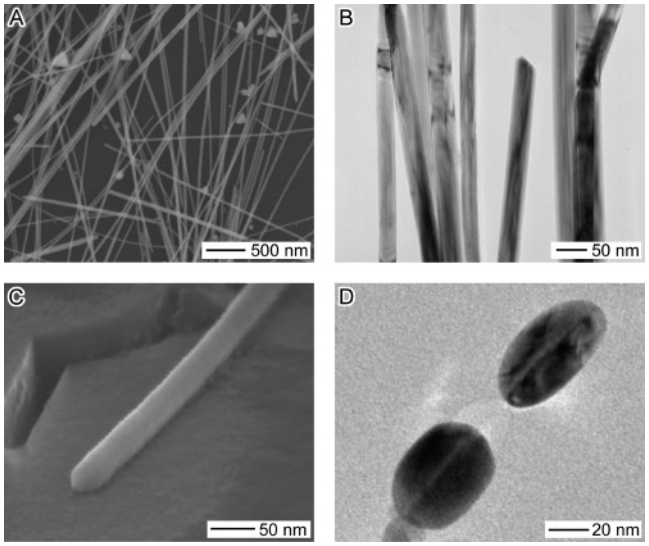

Figure 5. (A) SEM and (B) TEM images of Ag nanobeams indicating that they were narrower than pentagonal nanowires. (C) SEM image of a nanobeam tilted at 65° relative to the electron beam, where its rounded profile is visible. (The scale bar applies only to the horizontal axis.) (D) TEM image of a microtomed sample of Ag nanobeams showing their cross-sectional profile. This image suggests that the nanobeam is bisected by a twin plane parallel to the base.

Seeds with only a single twin can be produced and grown to form silver nanobeams when silver nitrate is reduced by ethylene glycol in the presence of PVP and bromide.[27] Bromide, being less corrosive than chloride, causes moderate etching that is sufficient to remove multiply twinned decahedrons but leaves seeds with a single twin intact. A relatively low rate of atomic addition to singly twinned seeds caused them to grow anisotropically and form silver nanobeams after 24 h. Figure 5A is an SEM image of the silver nanobeams, 85% of which are less than 40 nm in width. Figure 5B shows a TEM image in which nanobeams displayed striations of contrast that were quite distinct from the 2-fold contrast characteristic of pentagonal nanowires. This contrast may result from slight bending and/or twisting of the nanobeams. After tilting the sample normal by 65°, we could resolve the rounded, cross-sectional profile of an individual nanobeam (Figure 5C). Figure 5D gives a TEM image of the microtomed cross-sections of two nanobeams. Both appear to be bisected by a single twin plane, suggesting that the nanobeams indeed grew from singly twinned seeds. The nanobeam in the lower left of this image, which appears to be more closely aligned with the electron beam, is 38 nm wide and 27 nm thick with a width-to-thickness ratio W/T of 1.4. The name of the nanobeam results from the similarity of this W/T to a beam of wood.

It is possible that a capping agent other than PVP could produce nanostructures bound primarily by {111} facets.[28] We have found that sodium citrate could promote the formation of triangular nanoplates (95%) and nanobelts (5%). The nanobelts could be easily separated from the nanoplates by centrifugation. As shown in Figure 6A, these nanobelts have uniform lateral dimensions with a mean width of ∼9 nm, smooth surfaces, and lengths of up to 25 μm. The inset shows a typical SAED pattern taken from an individual nanobelt when the electron beam was oriented perpendicular to the TEM grid. The outer spots correspond to Bragg diffraction from the {220} lattice planes of silver, confirming that the wider side surfaces of the belts are composed

(26) (a) Johnson, C. J.; Dujardin, E.; Davis, S. A.; Murphy, C. J.; Mann, S. *J. Mater. Chem.* **2002**, *12*, 1765. (b) Lisiecki, I.; Filankembo, A.; Sack-Kongehl, H.; Weiss, K.; Pileni, M.-P.; Urban, J. *Phys. Rev. B* **2000**, *61*, 4968.

(27) Wiley, B. J.; Wang, Z.; Wei, J.; Yin, Y.; Cobden, D. H.; Xia, Y. *Nano Lett.* **2006**, *6*, 2273.

(28) Sun, Y.; Mayers, B.; Xia, Y. *Nano Lett.* **2003**, *3*, 675.

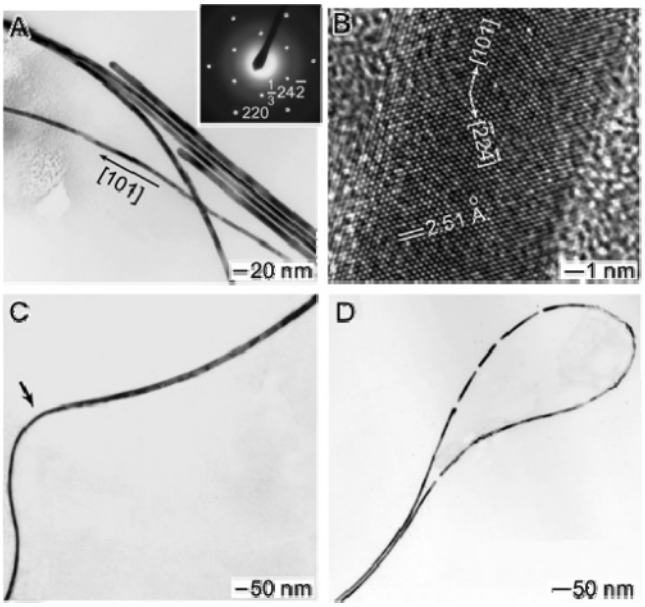

Figure 6. (A) TEM image of Ag nanobelts, with the inset showing a typical ED pattern taken from an individual nanobelt. (B) High-resolution TEM image of a nanobelt indicating that the nanobelt grew along the [101], together with a highly crystalline structure. (C) TEM image of an individual nanobelt showing a twisting in the middle portion, whereby its width can be measured. (D) TEM image of a Ag nanobelt ~10 nm in diameter that broke into short segments during sample preparation.

of {111} planes. The inner spots could be ascribed to the (1/3){422} reflection. This forbidden reflection has also been observed for Ag or Au nanostructures in the form of thin plates bounded by atomically flat surfaces as well as for nanoplates with internal stacking faults.[21] Figure 6B gives a typical HRTEM image of a nanobelt, indicating that the growth of this nanobelt occurred along the [101] axis. Figure 6C shows the TEM image of a nanobelt ~25 nm in width that was twisted in the middle. As limited by Rayleigh instability,[29] 1-D nanostructures tend to break into shorter segments when their lateral dimensions decrease below a critical value. Figure 6D shows the TEM image of a 10 nm Ag nanobelt that had broken into segments along its longitudinal axis as a result of thermal fluctuations. This observation suggests that the mechanical and thermal stability of metal nanowires or nanobelts is an important factor in determining their use as interconnects in fabricating electronic devices. In principle, 1-D nanostructures of metals can be coated with conformal sheaths made of silica or other dielectric materials to enhance their thermal and mechanical stability substantially.

Kinetically Controlled Growth of Platinum Nanorods, Nanowires, and Multipods. In a recent study,[30] we discovered that single-crystal Pt nanorods can be obtained by manipulating the reduction kinetics of a polyol process through the addition of a trace amount of iron species (Fe^{2+} or Fe^{3+}) to the reaction system. In a typical polyol process, H_2PtCl_6 is added to and reduced by ethylene glycol in the presence of PVP at 110 °C. The reduction mechanism involves the formation of Pt(II) species as an intermediate, which can exist for several months at room temperature. When the reaction is allowed to proceed at 110 °C, the reduction of Pt(II) species will be greatly accelerated via an autocatalytic process once Pt(0) nuclei have formed in the solution.[31] In this case, Pt spherical nanoparticles with a mean diameter of ~5 nm are obtained as the final product in 1 h. It is worth pointing out that the spherical shape is favored in the context of thermodynamics for an fcc metal.

By introducing a trace amount of Fe^{2+} or Fe^{3+} species and/or nitrogen at 110 °C, the reduction kinetics can be manipulated to obtain Pt nanostructures with different morphologies, including uniform nanorods and branched multipods. Figure 7 summarizes all of the major products that we have obtained under different reaction conditions. The reduction of Pt(II) to Pt(0) becomes slower in air than under nitrogen, suggesting that the adsorption of oxygen from air onto the surface of Pt nuclei is capable of slowing down the autocatalytic reduction of Pt(II) species.[32] Although the presence of oxygen can substantially slow down this process, the reduction is still too fast to induce the formation of any anisotropic nanostructure. In contrast, the reduction of Pt(II) species dwindles when a trace amount of Fe^{2+} or Fe^{3+} species is introduced into the reaction mixture. In this case, Fe^{3+} oxidizes both Pt atoms and nuclei back to Pt(II) species, significantly reducing the concentration of Pt atoms in the solution. Because the resultant Fe^{2+} can be recycled back to Fe^{3+} by oxygen, both Fe^{2+} and Fe^{3+} species show the same function in controlling the reduction kinetics, and thereby only a trace amount of Fe^{3+} or Fe^{2+} species is needed for kinetic control. Through a combination of surface blocking and oxidative etching, the reduction rate of Pt(II) species can be adjusted to decrease in order from product A to product E in Figure 7. As the reduction rate becomes slower, the addition of Pt atoms to the seed preferentially occurs along the [111] axis, leading to the formation of highly anisotropic, 1-D, or branched nanostructures.

Figure 8A shows a typical SEM image of product E, micrometer-sized agglomerates of Pt nanoparticles with surfaces covered by a densely packed array of Pt nanorods (inset). To examine the hierarchical structure further, Figure 8B gives a TEM image of a microtomed agglomerate resembling a sea urchin. The inset shows a blown-up view of the portion indicated with a box. Nanorods cover the outer surface of this agglomerate with a thickness of ~100 nm whereas the interior contains nanoparticles. After brief sonication, the nanowires were released from the surface of the agglomerate. Figure 8C shows a typical TEM image of Pt nanorods that are ~5 nm in diameter. The inset gives a SAED pattern, with the four rings indexed to the {111}, {200}, {220}, and {311} diffractions corresponding to fcc Pt. Figure 8D shows a HRTEM image recorded from the end of a single Pt nanorod, indicating that the Pt nanowire grew along the [111] direction.

Most recently, we further modified this synthesis to control the Pt nanostructures better. In one demonstration,[33] we obtained Pt nanowires with controllable lengths by using spherical aggregates of Pt nanoparticles as substrates and by adding different amounts of H_2PtCl_6 to the reaction mixture. The spherical aggregates were prepared under the direction of an organic surfactant such as sodium dodecylsulfate (SDS). As an immediate advantage over the previously demonstrated system, the spherical aggregates are more uniform in size and shape and can be more than 5 times smaller in dimensions. As a result, these spherical aggregates provided a larger surface area for the nucleation and growth of Pt nanorods and then nanowires (Figure 8E). The Pt nanowires could be separated from the substrates through a combination of brief sonication and centrifugation. The spherical

(29) Quere, D.; Meglio, J.-M. D.; Brochard-Wyart, F. *Science* **1990**, *249*, 1256.
(30) Chen, J.; Herricks, T.; Geissler, M.; Xia, Y. *J. Am. Chem. Soc.* **2004**, *126*, 10854.
(31) Petroski, J. M.; Wang, Z.; Green, T. C.; El-Sayed, M. A. *J. Phys. Chem. B* **1998**, *102*, 3316.
(32) Mallat, T.; Baiker. A. *Catal. Today* **1994**, *19*, 247.
(33) Chen, J.; Xiong, Y.; Yin, Y.; Xia, Y. *Small* **2006**, *2*, 1340.

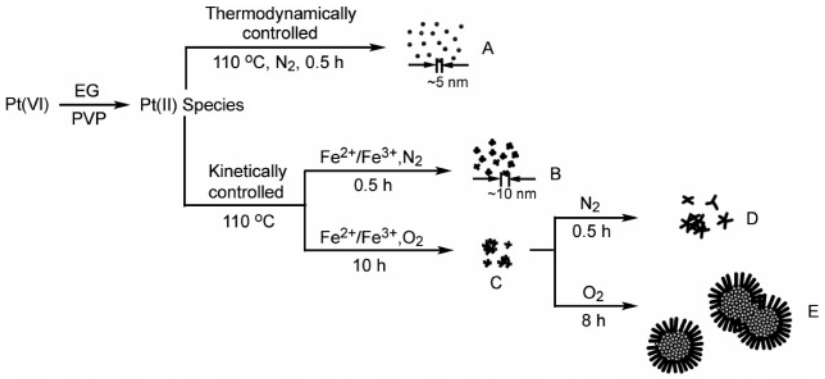

Figure 7. Schematic detailing all of the major steps and conditions for controlling the reduction kinetics of a Pt(IV) precursor by ethylene glycol (EG) and the corresponding morphologies observed for the Pt nanostructures: (A) spheres; (B) stars; (C, D) multiple pods; and (E) rods on aggregates of Pt nanoparticles.

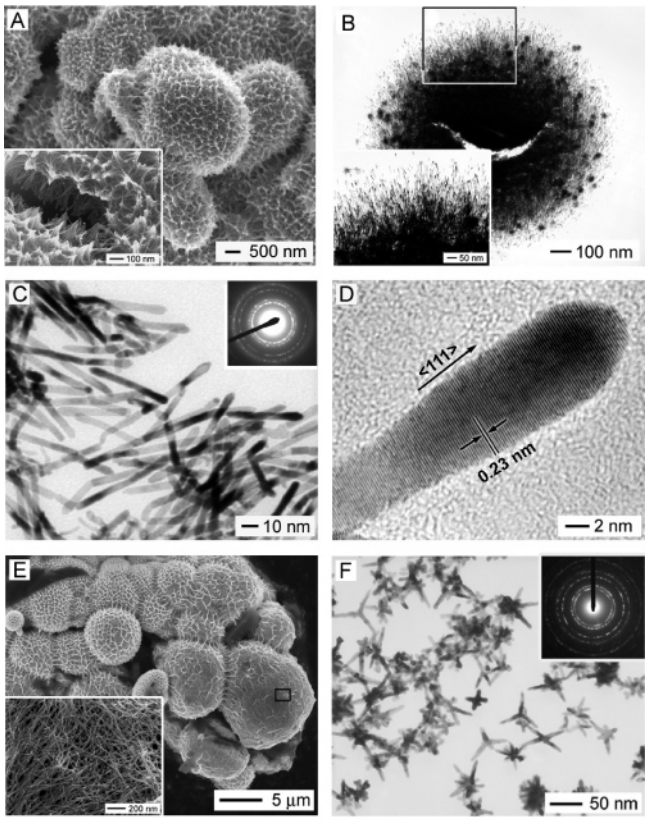

Figure 8. (A) SEM images of the hierarchically structured Pt agglomerates shown in Figure 7E. The inset shows the surface of these agglomerates covered by a thin layer of Pt nanorods. (B) Cross-sectional TEM image of a microtomed sample. The inset is an enlarged TEM image of the boxed region indicating that the Pt nanorods are uniaxially aligned in the plane of cleavage as a result of the shear force induced by the diamond knife. (C) TEM image and electron diffraction pattern of Pt nanowires that had been released from the surface of agglomerates via sonication. (D) HRTEM image of the tip of an individual Pt nanowire indicating that it was a single crystal, with its growth direction along the [111] axis. (E) SEM images of Pt nanowires formed on the surface of Pt agglomerates. The inset shows an enlarged image of Pt nanowires as indicated in the box. (F) TEM image and (inset) ED pattern of Pt multipods—product D in Figure 7.

aggregates could then be reused as substrates for additional rounds of nanowire growth. In a related work,[34] we demonstrated that dense coatings of Pt nanoparticles or Pt nanowires could be directly grown on Pd-coated colloidal spheres made of silica or polymer. The use of a polymeric or ceramic sphere as the substrate provides a more cost-effective procedure for growing Pt nanowires than the previous demonstrations where aggregates of Pt nanoparticles served as the substrates. The Pt nanowires and the coating of Pt nanoparticles could be extended to 200 nm long and up to 100 nm thick, respectively. After coating, the colloidal spheres could be selectively etched away to leave behind shells of Pt nanowires. These new methods can potentially be adapted to flat substrates of ceramic and polymeric materials for various technical applications.

In addition to Pt nanorods and nanowires, it is also possible to generate Pt multipods by fine tuning the reduction kinetics.[35] As shown in Figure 7, the product of a polyol synthesis can display a range of different morphologies depending on whether the polyol synthesis was conducted under air or nitrogen. If the reaction was allowed to proceed under nitrogen, star-shaped nanoparticles (product B) were obtained over a period of 1 h. If the reduction was continued in air, then it proceeded at a much slower rate and the nanostructures became more branched and subsequently assembled into submicrometer-sized agglomerates (product C). Toward the end of this reaction, the Pt(II) species would be reduced at an extremely slow rate to generate uniform Pt nanowires (product E) on the surface of each agglomerate. However, if nitrogen was applied, then the reduction rate would be slightly increased, resulting in the formation of branched multipods (product D).[36] Figure 8F shows a TEM image of the product that was obtained when the Pt(II) intermediate was heated in air for 10 h, followed by nitrogen protection for 1 h. The resultant nanostructures branched into multipods with an overall dimension on the scale of 50 nm. In the current stage of development, the final product of a typical synthesis is usually a mixture of multipods containing two to six arms. Some of them are single crystals, and others may contain twin defects. For the tetrahedral configuration, we believe that there is only one single-crystal seed involved and the four arms simply grow out of different sites (four of the eight corners) of the seed along the ⟨111⟩ directions. The kinetic control of reduction through oxygen adsorption and etching by an inorganic redox pair has also been extended from Pt to other noble metals such as Pd and Rh.[37]

(34) Lee, E. P.; Chen, J.; Yin, Y.; Campbell, C. T.; Xia, Y. *Adv. Mater.* **2006**, *18*, 3271.
(35) Chen, J.; Herricks, T.; Xia, Y. *Angew. Chem., Int. Ed.* **2005**, *44*, 2589.
(36) Teng, X.; Yang, H. *Nano Lett.* **2005**, *5*, 885.
(37) (a) Xiong, Y.; Chen, J.; Wiley, B.; Xia, Y.; Aloni, S.; Yin, Y. *J. Am. Chem. Soc.* **2005**, *127*, 7332. (b) Xiong, Y.; Chen, J.; Wiley, B.; Xia, Y.; Yin, Y.; Li, Z.-Y. *Nano Lett.* **2005**, *5*, 1237. (c) Xiong, Y.; McLellan, J.; Chen, J.; Yin, Y.; Li, Z.-Y.; Xia, Y. *J. Am. Chem. Soc.* **2005**, *127*, 17118. (d) Xiong, Y.; Wiley, B.; Chen, J.; Li, Z.-Y.; Yin, Y.; Xia, Y. *Angew. Chem., Int. Ed.* **2005**, *44*, 7913. (e) Zettsu, N.; McLellan, J.; Wiley, B.; Yin, Y.; Li, Z.-Y.; Xia, Y. *Angew. Chem., Int. Ed.* **2005**, *45*, 1288.

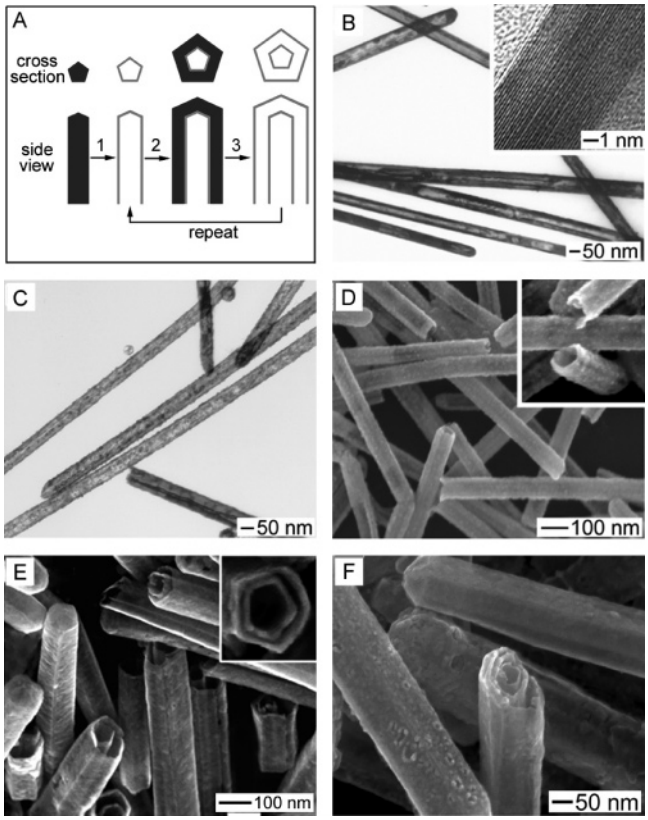

Figure 9. (A) Schematic of the experimental procedure used to fabricate metal nanotubes with coaxial multiple walls: Steps 1 and 3 involve the template-engaged replacement reaction between Ag and a metal (Au, Pt, or Pd) salt whereas step 2 involves electroless plating of silver. Multiple-walled nanotubes can be obtained by repeating steps 2 and 3. (B) SEM image of Au−Ag alloy nanotubes obtained by reacting Ag nanowires with aqueous $HAuCl_4$. The inset gives a high-resolution TEM image of the nanotubes. (C) TEM image of Pt−Ag nanotubes showing that the walls were composed of discrete nanoparticles. (D) SEM image of Pd−Ag nanotubes with the inset showing the open end of a nanotube. (E, F) SEM images of double- and triple-walled nanotubes made of Au−Ag alloys, respectively.

Template-Directed Synthesis of Gold, Palladium, and Platinum Nanotubes. The galvanic replacement reaction between two metals can be used to transform Ag nanowires into nanotubes made of other noble metals.[38] To this end, we have successfully synthesized highly crystalline single- and multiple-wall nanotubes consisting of noble metals such as Au, Pd, and Pt. Figure 9A outlines all of the major steps involved in the synthesis of such nanotubes. The sacrificial template—Ag nanowires with a pentagonal cross-section—were synthesized through the polyol process.[24] When Ag nanowires are mixed and boiled with an aqueous $HAuCl_4$ solution, their surface will be oxidized to generate silver ions. At the same time, the electrons released from this oxidation reduce $HAuCl_4$ to gold atoms. Thanks to a good matching of lattice spacing for gold and silver, the gold atoms will be epitaxially deposited on the surface of the Ag nanowire, leading to the formation of a conformal sheath (step 1). In step 2, the resultant nanotube is coated with a conformal thin layer of Ag through an electroless plating process. After the galvanic replacement reaction is repeated (step 3), a double-walled nanotube will be formed. By repeating steps 2 and 3, a coaxial multiple-wall nanotube can be obtained.

In principle, the silver-engaged replacement reaction can be applied to any metal whose redox potential is higher than that of the Ag^+/Ag pair (0.80 V vs SHE), such as the Au^+/Au pair (1.8 V vs SHE), the Pt^{2+}/Pt pair (1.2 V vs SHE), and the Pd^{2+}/Pd pair (0.95 V vs SHE). Figure 9B shows a TEM image of Au/Ag alloy nanotubes obtained by refluxing Ag nanowires with an aqueous solution of $HAuCl_4$. The nanotubes were composed of gold and silver with an atomic ratio of 4:1. The inset gives a HRTEM image recorded from the edge of an individual nanotube, indicating that the Au and Ag had formed an alloy rather than a heterogeneous or mosaic structure. The alloying process occurs at 100 °C for two reasons: (i) the high diffusion coefficients of Ag and Au atoms and (ii) the high thermodynamic stability of a homogeneous Au/Ag alloy relative to that of a mixture of Au or Ag.[39] Compared with Au/Ag nanotubes, the walls of Pt/Ag nanotubes were rougher and primarily composed of discrete nanoparticles (Figure 9C). The difference between Au and Pt can be attributed to the higher melting point of Pt and the lattice mismatch between Pt and Ag (∼4.1%). Figure 9D shows an SEM image of Pd/Ag nanotubes with continuous and smooth sheaths obtained by refluxing Ag nanowires with an aqueous $Pd(NO)_3$ solution. In this case, the precursor solution must be freshly prepared before use to prevent the hydrolysis of Pd cations to form $Pd(OH)_2$, which is unable to oxidize Ag to Ag^+. The inset gives an SEM image of the Pd/Ag nanotubes after brief sonication, confirming that they were hollow with a uniform wall thickness. Parts E and F of Figure 9 show SEM images of double- and triple-wall Au/Ag nanotubes obtained by repeating steps 2 and 3 in Figure 8 two and three times, respectively. These nanotubes of metals with controllable sizes, structures, compositions, and morphologies are expected to find use in applications including catalysis, gas storage, optoelectronics, electronics, and optical sensing.

Transport Properties of 1-D Nanostructures of Metals

Transport Measurements of Silver Nanobeams. One-dimensional nanostructures of silver are promising nanoscale conduits for electricity or heat because bulk silver has the highest electrical and thermal conductivity among all metals.[40] It is therefore important to determine down to what scale individual nanostructures of silver retain the excellent properties of the bulk material. The minute dimensions, smooth surface, and crystallinity of Ag nanobeams make them promising candidates for studying the effects of size on electron transport. To make electrical contact with a single nanobeam, an aqueous suspension of nanobeams was dried over gold contacts on an oxidized silicon substrate (Figure 10A).[27] Figure 10B shows a nanobeam that is 27 nm wide and 19 nm thick spanning gold contacts separated by 1.5 μm. To ensure metal-to-metal contact, the ends of the nanobeam were annealed to the gold with a focused electron beam, causing slight deformation as can be seen in the inset magnified images of Figure 10B.

We measured a collection of nanobeams with different lengths L and widths W (with $W/T \approx 1.4$ for all) to investigate the effect of size on their resistivity and current-carrying ability. The effective resistivity ρ of a uniform metal film or wire will be higher than the bulk value ρ_0 as a result of surface scattering. If we take wires of a given cross-sectional shape and consider reducing the cross-sectional area $A \equiv a^2$, then the correction to

(38) (a) Sun, Y.; Wiley, B.; Li, Z.-Y.; Xia. Y. *J. Am. Chem. Soc.* **2004**, *126*, 9399. (b) Sun, Y.; Xia, Y. *Adv. Mater.* **2004**, *16*, 264. (c) Sun, Y.; Tao, Z.; Chen, J.; Herricks, T.; Xia, Y. *J. Am. Chem. Soc.* **2004**, *126*, 5940. (d) Sun, Y.; Mayers, B.; Xia, Y. *Adv. Mater.* **2003**, *15*, 641. (e) Sun, Y.; Mayers, B.; Xia, Y. *Nano Lett.* **2002**, *2*, 481.

(39) Sun, Y.; Xia, Y. *J. Am. Chem. Soc.* **2004**, *126*, 3892.

(40) Carmon, F.; Barreau, F.; Delhaes, P.; Canet, R. *J. Phys., Lett.* **1980**, *41*, L-531.

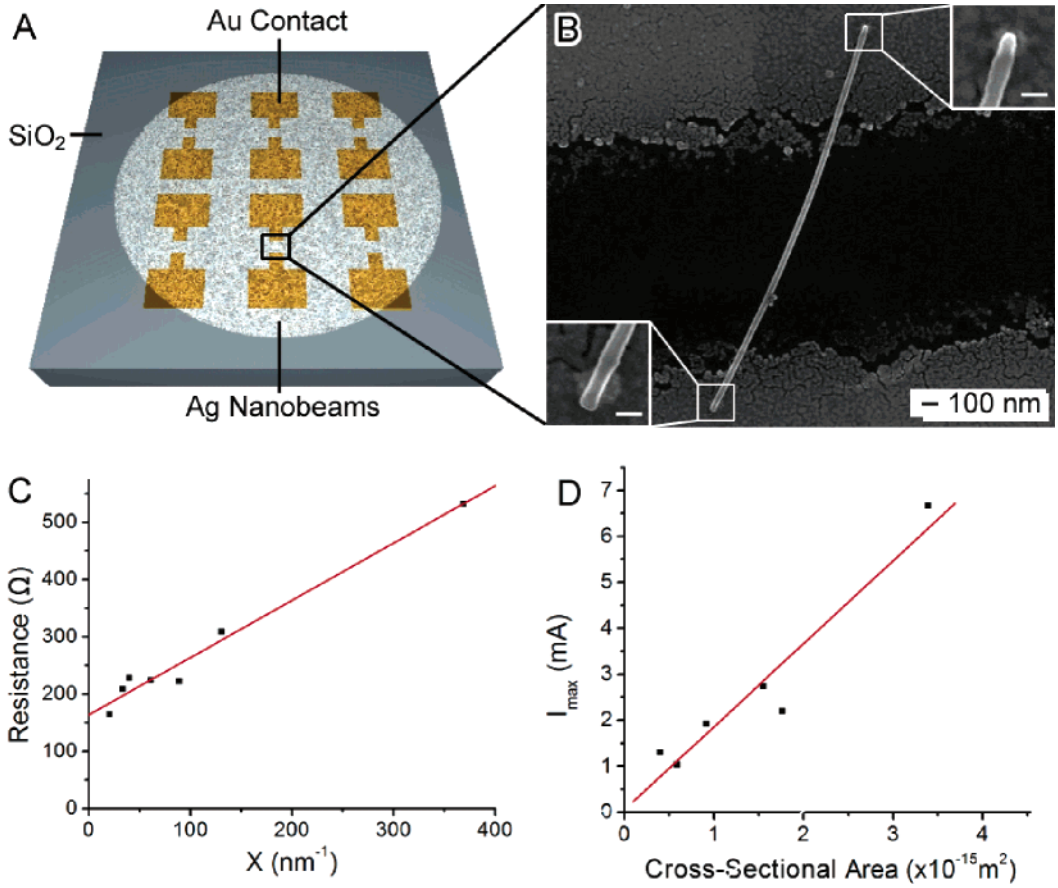

Figure 10. (A) Silver nanobeams deposited from solution onto gold contacts. (B) SEM image of a single nanobeam that is 27 nm wide and 19 nm high spanning the gap across the gold contacts. Insets show the deformation resulting from annealing the ends to the contacts with a focused electron beam (scale bar 50 nm). (C) Plot of resistance vs $X = \rho_0 L/0.56W^2(1 + (\lambda/0.75W))$ for seven nanobeams using $\lambda = 15$ nm. The straight-line fit has a slope of unity, and the y intercept gives a contact resistance of $R_c = 164\ \Omega$. (D) The current at failure, I_{max}, is roughly proportional to the cross-sectional area of the nanobeams.

ρ should initially be linear in the surface-to-volume ratio a^{-1} (i.e., $\rho = \rho_0(1 + {}^{\lambda}/_{a})$, where λ is a characteristic length scale and ${}^{\lambda}/_{a} \ll 1$).[41] The scale λ is set by the bulk mean free path l, the shape, and the details of the surface scattering. In addition to the bulk resistance of the nanobeam, we anticipate a contact resistance R_c. Assuming for simplicity that R_c is the same for every device and using $A \approx \pi WT/4 \approx 0.56W^2$ and $a = A^{1/2} \approx 0.75W$ for the nanobeams, we obtain

$$R - R_c \approx \rho\frac{L}{A} \approx \rho_0\frac{L}{0.56W^2}\left(1 + \frac{\lambda}{0.75W}\right) \qquad (1)$$

To determine how well this describes the nanobeams, we plotted values of R against values of the expression on the right-hand side of eq 1 calculated using the bulk value of $\rho_0 = 1.6\ \mu\Omega$ cm for silver and a value of λ that was adjusted to give the best fit to a straight line of slope unity. The result is shown in Figure 10C, with $\lambda = 15$ nm and a best fit straight line giving $R_c = 164\ \Omega$. We deduce that the data is consistent with eq 1. The scatter about the straight line can be explained by random variations in the resistance of the contacts. It appears that the nanobeams largely retain the unparalleled electrical conductivity of bulk silver. According to eq 1, even our thinnest nanobeams, with a width of 20 nm, have a resistivity that is only twice that of bulk silver.

We determined the maximum current that the nanobeams can support by plotting the current at failure, I_{max}, versus cross-sectional area A in Figure 10D. The data is consistent with $I_{max} \propto A$ with a slope representing a well-defined maximum current density of approximately 1.8×10^8 A cm^{-2}. This is comparable to the highest current densities reported for multiwalled carbon nanotubes ($\sim 10^9$ A cm^{-2}).[42] These consistent and predictable characteristics, in addition to the ease with which they can be

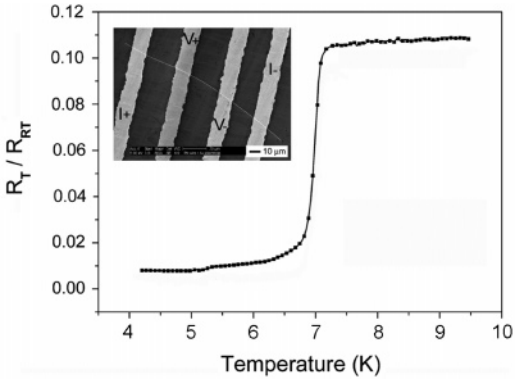

Figure 11. Plot illustrating the dependence of resistance on temperature for an individual Pb nanowire. The resistance was normalized against the data taken at room temperature. The inset shows an SEM image of the typical setup used for the four-probe transport measurement, where a single Pb nanowire was deposited on the four gold electrodes equally separated by 25 μm. The electrodes denoted by I+ and I− were used as sources for current feeding whereas V+ and V− were used to measure the potential drop. The resistances of this Pb nanowire exhibited a clear transition to the superconducting state at a critical temperature similar to that of bulk lead.

(41) Dingle, R. B. *Proc. R. Soc. London, Ser. A* **1950**, *201*, 545.

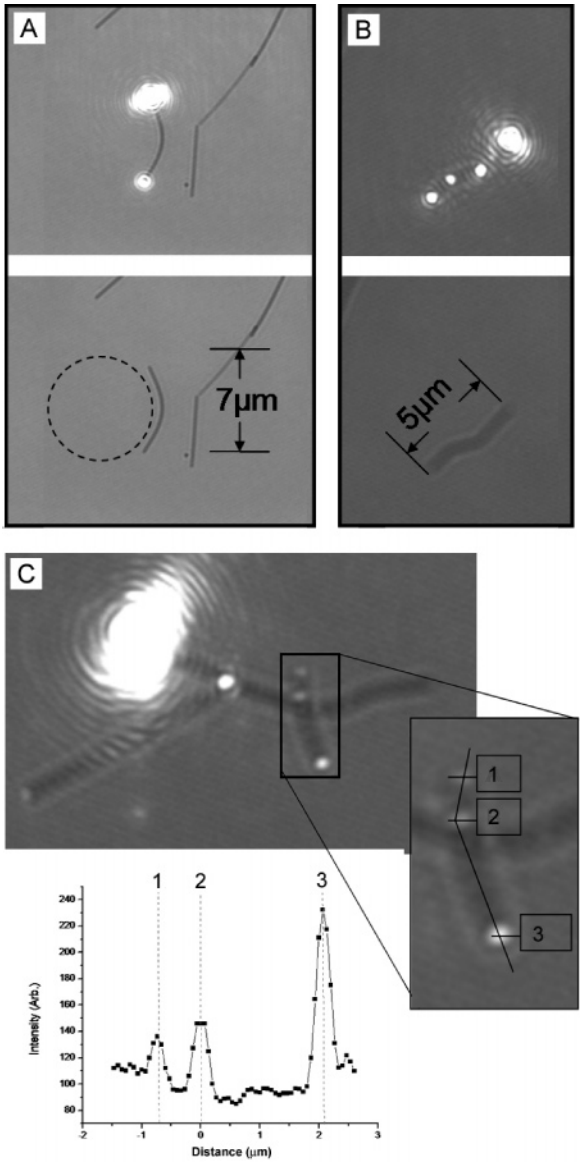

Figure 12. Optical micrographs showing plasmon excitation, propagation, and emission in Ag nanowires. The brightest point in each image is scattered light from the incident laser. (A) Light propagated as a plasmon along a 7 μm wire with a radius of curvature of 4 μm and emitted from the other end. (B) The sharp kinks in a 5 μm wire caused radiation of light in addition to that at the end. (C) The excitation at the far left end of a nanowire produces emission at both the junctions and ends of adjacent, coupled nanowires. The inset gives the emission intensity profile along the nanowire.

grown and handled, make silver nanobeams a competitive option for use as electrical interconnects.

Superconductivity of Lead Nanowires. It is well known that lead is a superconductor and its bulk resistance drops to zero at a critical temperature of 7.2 K. Several other groups have observed the transition from metal to superconductor for Pb nanowires prepared by templating against channels in porous membranes.[43] However, all of these measurements were performed on an array of nanowires by directly contacting the top and bottom surfaces of a membrane template. Therefore, the measured resistance was an averaged response from a large number of nanowires that were inevitably different in diameter and crystallinity. Michotte and co-workers reported their study on the electron-transport properties of individual Pb nanowires with a clever design, but the nanowire was still embedded in the pore of the polycarbonate membrane used for electrochemical deposition.[44] By taking advantage of single-crystal Pb nanowires prepared using the solution-based synthesis, our group was able to measure the electron-transport properties of individual Pb nanowires with uniform diameters without the involvement of a template.

We studied the electron-transport properties of the as-synthesized Pb nanowires using the four-probe technique.[19] The contacts in the measurement (inset in Figure 11) were made by depositing a single lead nanowire through solvent evaporation on the four gold electrodes that had been patterned on a glass slide, followed by thermally annealing the regions in physical contact via brief exposure to the electron beam of a scanning electron microscope. Because of the low melting point of Pb, the current used in all measurements was kept below 1.5 μA to avoid melting the nanowires. At room temperature, the resistance of a Pb nanowire was measured in the range from hundreds of ohms to several kilohms depending on the lateral dimensions of the lead nanowire. As the temperature decreased, the resistance dropped continuously. Figure 11 shows a plot of the resistance (in the form of R_T/R_{RT}) as a function of temperature for a Pb nanowire that is 50 nm in diameter. When the temperature was reduced to 7 K, there was a sharp drop in resistance, indicating that the nanowire had entered the superconducting state. As the temperature was further decreased, R_T/R_{RT} continued to decrease but at a slower rate. Note that the resistance never dropped to zero in all of our measurements, which might be due to the fact that the resistive heating could slowly transform the wire surface to a thin layer of lead oxide at temperatures above the transition temperature. It has been shown in previous studies that the transition temperature decreased as the diameter of the nanowires was reduced, suggesting that the introduction of disorder into a nanowire weakens the superconducting property.[45] For all Pb nanowires with diameters down to ~50 nm, we did not observe any significant difference in their critical transition temperatures, and the critical temperature was found to be similar to the value reported for bulk lead.

Plasmon Propagation in Silver Nanowires

Nanoscale optical circuits and sensors require a way to guide, redirect, and focus light on scales smaller than the free-space wavelength.[46] This has been realized by coupling photons to plasmons—fluctuations in the density of electrons on the surface of a metal—but complex coupling mechanisms or structures fabricated through electron beam lithography were required. Recently, through collaboration with Mark Reed's group at Yale University, we demonstrated a simple approach to observe the propagating plasmon modes in chemically synthesized Ag nanowires.[47]

Plasmons were launched by illuminating one end of a single Ag nanowire with a diffraction-limited laser spot. The momentum of the incoming photon (k_{photon}) is not matched to that of the

(42) (a) Bourlon, B.; Glattli, D. C.; Placais, B.; Berroir, J. M.; Milko, C.; Forro, L.; Bachtold, A. *Phys. Rev. Lett.* **2004**, *92*, 026804. (b) Wei, B. Q.; Vajtai, R.; Ajayan, P. M. *Appl. Phys. Lett.* **2001**, *79*, 1172.

(43) (a) Dubois, S.; Michel, A.; Eymery, J.; Duvail, J.; Piraux, L. *J. Mater. Res.* **1999**, *14*, 665. (b) Michotte, S.; Piraux, L.; Dubois, S.; Pailloux, F.; Stenuit, G.; Govaerts, J. *Physica C* **2002**, *377*, 267. (c) Yi, G.; Schwarzacher, W. *Appl. Phys. Lett.* **1999**, *74*, 1746.

(44) (a) Michotte, S.; Matefi-Tempfli, S.; Piraux, L. *Appl. Phys. Lett.* **2003**, *82*, 4119; (b) Michotte, S.; Matefi-Tempfli, S.; Piraux, L. *Physica C* **2003**, *391*, 369.

(45) (a) Graybeal, J.; Mankiewich, P.; Dynes, R.; Beasley, M. *Phys. Rev. Lett.* **1987**, *59*, 2697. (b) Sharifi, F.; Herzog, A.; Dynes, R. *Phys. Rev. Lett.* **1993**, *71*, 428. (c) Herzog, A.; Xiong, P.; Sharifi, F.; Dynes, R. *Phys. Rev. Lett.* **1996**, *76*, 668.

(46) Xia, Y.; Halas, N. J. *MRS Bull.* **2005**, *30*, 338.

(47) Sanders, A. W.; Routenberg, D. A.; Wiley, B. J.; Xia, Y.; Dufresne, E. R.; Reed, M. A. *Nano Lett.* **2006**, *6*, 1822.

propagating plasmon ($k_{plasmon}$), so scattering is required to provide an additional wavevector ($\Delta k_{scatter}$). This condition is met at the ends of the nanowire, where light can scatter axially into propagating plasmon modes. As shown in Figure 12A, once light is coupled into the nanowire it can navigate around tight bends with a radius of curvature of 4 μm before reemitting at the opposite end. Kinks with radii of curvature of less than 1 μm act as additional scattering centers, causing light to leak out of the nanowire pictured in Figure 12B. In comparison, a good single-mode optical fiber shows significant bend loss for radii of curvature below ~500 μm.

Directing the laser at the end of a nanowire in contact with others causes the propagating modes to couple between them. As shown in Figure 12C, emission was observed not only at the intersections between nanowires in contact with the one irradiated by the laser but also at their ends, suggesting that this system can produce plasmon fan-out. As indicated by the inset in Figure 12C, the intensity of the emitted light is mainly determined by the coupling coefficient rather than nanowire length. Thus, using a simple far-field excitation method, we have demonstrated that Ag nanowires can guide light around tight bends as well as couple light to adjacent Ag nanowires. These plasmon-based nanoscale waveguides will allow the miniaturization of optical devices to scales that are smaller than the free-space wavelength of light.

Conclusion and Perspectives

We have demonstrated a number of synthetic approaches by which 1-D nanostructures of Pb, Ag, and Pt can be produced in large quantities through the guided assembly of atoms in solution. Nanotubes composed of Au, Pd, and Pt have also been synthesized in solution phase by using Ag nanowires as a sacrificial template. The analysis of each metal nanostructure demonstrates how the characteristic chemical and physical properties of different metals translate to the nanoscale. Low-temperature conductivity measurements of Pb nanowires with diameters down to 50 nm show critical transition temperatures that are not different from those of the bulk. Electrical measurements on Ag nanobeams demonstrate that they retain the low resistivity of bulk silver for thicknesses down to ~15 nm and their current-carrying capacity is comparable to the highest value reported for multiwalled carbon nanotubes. Last, we have illustrated how plasmon propagation through pentagonal Ag nanowires allows them to serve as nanoscale conduits for light.

Now that we have synthesized and characterized a variety of nanostructures, the last question comes into play: how can properties unique to nanostructures be exploited for applications? This will require a study of the performance of nanostructures in the context in which they will be used rather than in a laboratory environment. Blending nanostructures into other materials to make nanocomposites with new properties seems to be the most straightforward route to the utilization of nanostructures, but this has yet to be done for chemically synthesized 1-D nanostructures of metals. The major challenge here may be dispersing the 1-D nanostructures into a matrix and maintaining their integrity during the blending process.[48] Much greater attention has been given to using nanostructures in electronics,[49] photonics,[50] and sensing[51] and where the size, properties, and low cost of chemically synthesized nanostructures clearly give them an advantage over their counterparts fabricated through lithography. Although much progress has been made, it remains a challenge to pattern chemically synthesized nanostructures with the precision of lithography.[52] Considering the fact that the nanostructures discussed here did not exist 5 years ago, these unsolved issues and challenges should be viewed as opportunities for a contribution.

Acknowledgment. This work was supported in part by the NSF (DMR-0451788), a CAREER award from the NSF (DMR-9983893), an AFOSR-DURINT subcontract from SUNY-Buffalo, and a fellowship from the David and Lucile Packard Foundation. Y.X. was an Alfred P. Sloan Research Fellow (2000−2005) and is a Camille Dreyfus Teacher Scholar (2002−2007). J.C. was supported by a fellowship from the Center for Nanotechnology at the UW. B.W. thanks the UW Center for Nanotechnology for an IGERT fellowship funded by the NSF and NCI. This work used the Nanotech User Facility (NTUF) at the UW, a member of the National Nanotechnology Infrastructure Network (NNIN) supported by the NSF.

LA063193Y

(48) Hussain, F.; Hojjati, M.; Okamoto, M.; Gorga, R. E. *J. Compos. Mater.* **2006**, *40*, 1511.
(49) Sun, Y.; Khang, D.-Y.; Hua, F.; Hurley, K.; Nuzzo, R. G.; Rogers, J. A. *Adv. Funct. Mater.* **2005**, *15*, 30.
(50) (a) Li, Y.; Qian, F.; Xiang, J. Lieber, C. M. *Mater. Today* **2006**, *9*, 18. (b) Pauzauskie, P. J.; Yang, P. *Mater. Today* **2006**, *9*, 36.
(51) (a) Cui, Y.; Wei, Q.; Park, H.; Lieber, C. M. *Science* **2001**, *293*, 1289. (b) Favier, F.; Walter, E. C.; Zach, M. P. Benter, T.; Penner, R. M. *Science* **2001**, *293*, 2227.
(52) Xia, Y.; Rogers, J.; Paul, K.; Whitesides, G. M. *Chem. Rev.* **1999**, *99*, 1823.